Ultrafast and widely tuneable vertical-external-cavity surface-emitting laser, mode-locked by a graphene-integrated distributed Bragg reflector

C. A. Zaugg,[1*] Z. Sun,[2] V. J. Wittwer,[2] D. Popa,[2] S. Milana,[2] T. S. Kulmala,[2] R. S. Sundaram,[2] M. Mangold,[1] O. D. Sieber,[1] M. Golling,[1] Y. Lee,[3] J. H. Ahn,[3] A. C. Ferrari,[2] and U. Keller[1]

[1] *Department of Physics, Institute for Quantum Electronics, ETH Zürich, 8093 Zürich, Switzerland*

[2] *Cambridge Graphene Centre, University of Cambridge, Cambridge CB3 0FA, UK*

[3] *School of Electrical & Electronic Engineering, Yonsei University, Seoul 120-749 and SKKU Advanced Institute of Nanotechnology, Sungkyunkwan University, Suwon, 440-746, South Korea*

[*] *zauggc@phys.ethz.ch*

Abstract: We report a versatile way of controlling the unsaturated loss, modulation depth and saturation fluence of graphene-based saturable absorbers (GSAs), by changing the thickness of a spacer between a single layer graphene (SLG) and a high-reflection mirror. This allows us to modulate the electric field intensity enhancement at the GSA from 0 up to 400%, due to the interference of incident and reflected light at the mirror. The unsaturated loss of the SLG-mirror-assembly can be reduced to $\sim$0. We use this to mode-lock a vertical-external-cavity surface-emitting laser (VECSEL) from 935 to 981 nm. This approach can be applied to integrate SLG into various optical components, such as output coupler mirrors, dispersive mirrors or dielectric coatings on gain materials. Conversely, it can also be used to increase the absorption (up to 10%) in various graphene based photonics and optoelectronics devices, such as photodetectors.

OCIS codes: (140.7270) Vertical emitting lasers ; (140.4050) Mode-locked lasers; (140.5960) Semiconductor lasers; (160.4236) Nanomaterials; (160.4330) Nonlinear optical materials; (140.3600) Lasers, tunable.

References

1. U. Keller, "Recent developments in compact ultrafast lasers," Nature **424**, 831-838 (2003).
2. U. Keller and A. C. Tropper, "Passively modelocked surface-emitting semiconductor lasers," Phys. Rep. **429**, 67-120 (2006).
3. M. E. Fermann, A. Galvanauskas, and G. Sucha, *Ultrafast Lasers: Technology and Applications* (CRC Press, 2003).
4. T. Südmeyer, D. J. H. C. Maas, and U. Keller, "Mode-Locked Semiconductor Disk Lasers," in *Semiconductor Disk Lasers*, O.G. Okhotnikov, ed. (Wiley-VCH, 2010), pp. 213-261.
5. R. Aviles-Espinosa, G. Filippidis, C. Hamilton, G. Malcolm, K. J. Weingarten, T. Südmeyer, Y. Barbarin, U. Keller, S. I. C. O. Santos, D. Artigas, and P. Loza-Alvarez, "Compact ultrafast semiconductor disk laser: targeting GFP based nonlinear applications in living organisms," Biomed. Opt. Express **2**, 739-747 (2011).

#200054 - $15.00 USD Received 23 Oct 2013; revised 2 Dec 2013; accepted 2 Dec 2013; published 13 Dec 2013

6. K. G. Wilcox, A. C. Tropper, H. E. Beere, D. A. Ritchie, B. Kunert, B. Heinen, and W. Stolz, "4.35 kW peak power femtosecond pulse mode-locked VECSEL for supercontinuum generation," Opt. Express **21**, 1599-1605 (2013).
7. J. L. Jewell, J. P. Harbison, A. Scherer, Y. H. Lee, and L. T. Florez, "Vertical-cavity surface-emitting lasers: Design, growth, fabrication, characterization," IEEE J. of Quantum Electron. **27**, 1332-1346 (1991).
8. D. Lorenser, D. J. H. C. Maas, H. J. Unold, A.-R. Bellancourt, B. Rudin, E. Gini, D. Ebling, and U. Keller, "50-GHz passively mode-locked surface-emitting semiconductor laser with 100 mW average output power," IEEE J. of Quantum Electron. **42**, 838-847 (2006).
9. V. J. Wittwer, C. A. Zaugg, W. P. Pallmann, A. E. H. Oehler, B. Rudin, M. Hoffmann, M. Golling, Y. Barbarin, T. Südmeyer, and U. Keller, "Timing Jitter Characterization of a Free-Running SESAM Mode-locked VECSEL," IEEE Photonics Journal **3**, 658-664 (2011).
10. B. Rudin, V. J. Wittwer, D. J. H. C. Maas, M. Hoffmann, O. D. Sieber, Y. Barbarin, M. Golling, T. Südmeyer, and U. Keller, "High-power MIXSEL: an integrated ultrafast semiconductor laser with 6.4 W average power," Opt. Express **18**, 27582-27588 (2010).
11. B. Heinen, T. L. Wang, M. Sparenberg, A. Weber, B. Kunert, J. Hader, S. W. Koch, J. V. Moloney, M. Koch, and W. Stolz, "106 W continuous-wave output power from vertical-external-cavity surface-emitting laser," Electron. Lett. **48**, 516-517 (2012).
12. M. Scheller, T. L. Wang, B. Kunert, W. Stolz, S. W. Koch, and J. V. Moloney, "Passively modelocked VECSEL emitting 682 fs pulses with 5.1 W of average output power," Electron. Lett. **48**, 588-589 (2012).
13. C. J. Saraceno, C. Schriber, M. Mangold, M. Hoffmann, O. H. Heckl, C. R. E. Baer, M. Golling, T. Südmeyer, and U. Keller, "SESAMs for high-power oscillators: design guidelines and damage thresholds," IEEE J. Sel. Top. Quantum Electron. **18**, 29-41 (2012).
14. O. J. Morris, K. G. Wilcox, C. R. Head, A. P. Turnbull, P. J. Mosley, A. H. Quarterman, H. J. Kbashi, I. Farrer, H. E. Beere, D. A. Ritchie, and A. C. Tropper, "A wavelength tunable 2-ps pulse VECSEL," in *Photonics West*, (SPIE, 2012), pp. 824212.
15. M. Hoffmann, O. D. Sieber, V. J. Wittwer, I. L. Krestnikov, D. A. Livshits, Y. Barbarin, T. Südmeyer, and U. Keller, "Femtosecond high-power quantum dot vertical external cavity surface emitting laser," Opt. Express **19**, 8108-8116 (2011).
16. F. Bonaccorso, Z. Sun, T. Hasan, and A. C. Ferrari, "Graphene photonics and optoelectronics," Nat. Photonics **4**, 611 - 622 (2010).
17. R. R. Nair, P. Blake, A. N. Grigorenko, K. S. Novoselov, T. J. Booth, T. Stauber, N. M. R. Peres, and A. K. Geim, "Fine Structure Constant Defines Visual Transparency of Graphene," Science **320**, 1308-1308 (2008).
18. K. F. Mak, M. Y. Sfeir, Y. Wu, C. H. Lui, J. A. Misewich, and T. F. Heinz, "Measurement of the Optical Conductivity of Graphene," Phys. Rev. Lett. **101**, 196405 (2008).
19. D. Brida, A. Tomadin, C. Manzoni, Y. J. Kim, A. Lombardo, S. Milana, R. R. Nair, K. S. Novoselov, A. C. Ferrari, G. Cerullo, and M. Polini, "Ultrafast collinear scattering and carrier multiplication in graphene," Nature Comm. **4**, 1987 (2013).
20. A. Tomadin, D. Brida, G. Cerullo, A. C. Ferrari, and M. Polini, "Nonequilibrium dynamics of photoexcited electrons in graphene: Collinear scattering, Auger processes, and the impact of screening," Phys. Rev. B **88**, 035430 (2013).
21. F. Bonaccorso, A. Lombardo, T. Hasan, Z. Sun, L. Colombo, and A. C. Ferrari, "Production and processing of graphene and 2d crystals," Mater. Today **15**, 564-589 (2012).
22. Z. Sun, T. Hasan, and A. C. Ferrari, "Ultrafast lasers mode-locked by nanotubes and graphene," Physica E **44**, 1082-1091 (2012).
23. T. Hasan, Z. Sun, F. Wang, F. Bonaccorso, P. H. Tan, A. G. Rozhin, and A. C. Ferrari, "Nanotube-polymer composites for ultrafast photonics," Adv. Mater. **21**, 3874-3899 (2009).
24. Z. Sun, T. Hasan, F. Torrisi, D. Popa, G. Privitera, F. Wang, F. Bonaccorso, D. M. Basko, and A. C. Ferrari, "Graphene Mode-Locked Ultrafast Laser," ACS Nano **4**, 803-810 (2010).
25. I. H. Baek, H. W. Lee, S. Bae, B. H. Hong, Y. H. Ahn, D.-I. Yeom, and F. Rotermund, "Efficient mode-locking of sub-70-fs Ti:sapphire laser by graphene saturable absorber," Appl. Phys. Express **5**, 032701 (2012).
26. A. A. Lagatsky, Z. Sun, T. S. Kulmala, R. S. Sundaram, S. Milana, F. Torrisi, O. L. Antipov, Y. Lee, J. H. Ahn, C. T. A. Brown, W. Sibbett, and A. C. Ferrari, "2μm solid-state laser mode-locked by single-layer graphene," Appl. Phys. Lett. **102**, 013113 (2013).
27. R. Mary, G. Brown, S. J. Beecher, F. Torrisi, S. Milana, D. Popa, T. Hasan, Z. Sun, E. Lidorikis, S. Ohara, A. C. Ferrari, and A. K. Kar, "1.5 GHz picosecond pulse generation from a monolithic waveguide laser with a graphene-film saturable output coupler," Opt. Express **21**, 7943-7950 (2013).
28. M. Mangold, V. J. Wittwer, O. D. Sieber, M. Hoffmann, I. L. Krestnikov, D. A. Livshits, M. Golling, T. Südmeyer, and U. Keller, "VECSEL gain characterization," Opt. Express **20**, 4136-4148 (2012).
29. C. C. Lee, J. M. Miller, and T. R. Schibli, "Doping-induced changes in the saturable absorption of monolayer graphene," Appl. Phys. B **108**, 129-135 (2012).
30. F. Wang, Y. B. Zhang, C. S. Tian, C. Girit, A. Zettl, M. Crommie, and Y. R. Shen, "Gate-variable optical transitions in graphene," Science **320**, 206-209 (2008).

#200054 - $15.00 USD Received 23 Oct 2013; revised 2 Dec 2013; accepted 2 Dec 2013; published 13 Dec 2013

31. G. J. Spühler, K. J. Weingarten, R. Grange, L. Krainer, M. Haiml, V. Liverini, M. Golling, S. Schön, and U. Keller, "Semiconductor saturable absorber mirror structures with low saturation fluence," Appl. Phys. B **81**, 27-32 (2005).
32. B. E. A. Saleh and M. K. Teich, *Fundamentals of Photonics*, 2 ed. (John Wiley & Sons, Inc., 2007).
33. K. F. Renk, *Basics of Laser Physics* (Springer, 2012).
34. S. Bae, H. Kim, Y. Lee, X. Xu, J.-S. Park, Y. Zheng, J. Balakrishnan, T. Lei, H. Ri Kim, Y. I. Song, Y.-J. Kim, K. S. Kim, B. Ozyilmaz, J.-H. Ahn, B. H. Hong, and S. Iijima, "Roll-to-roll production of 30-inch graphene films for transparent electrodes," Nat. Nanotechnol. **5**, 574 - 578 (2010).
35. A. C. Ferrari, J. C. Meyer, V. Scardaci, C. Casiraghi, M. Lazzeri, F. Mauri, S. Piscanec, D. Jiang, K. S. Novoselov, S. Roth, and A. K. Geim, "Raman spectrum of graphene and graphene layers," Phys. Rev. Lett. **97**, 187401 (2006).
36. L. G. Cancado, A. Jorio, E. H. M. Ferreira, F. Stavale, C. A. Achete, R. B. Capaz, M. V. O. Moutinho, A. Lombardo, T. S. Kulmala, and A. C. Ferrari, "Quantifying defects in graphene via Raman spectroscopy at different excitation energies," Nano Lett. **11**, 3190-3196 (2011).
37. A. C. Ferrari and D. M. Basko, "Raman spectroscopy as a versatile tool for studying the properties of graphene," Nat. Nanotechnol. **8**, 235-246 (2013).
38. A. C. Ferrari and J. Robertson, "Interpretation of Raman spectra of disordered and amorphous carbon," Phys. Rev. B **61**, 14095-14107 (2000).
39. A. Das, S. Pisana, B. Chakraborty, S. Piscanec, S. K. Saha, U. V. Waghmare, K. S. Novoselov, H. R. Krishnamurthy, A. K. Geim, A. C. Ferrari, and A. K. Sood, "Monitoring dopants by Raman scattering in an electrochemically top-gated graphene transistor," Nat. Nanotechnol. **3**, 210-215 (2008).
40. V. G. Kravets, A. N. Grigorenko, R. R. Nair, P. Blake, S. Anissimova, K. S. Novoselov, and A. K. Geim, "Spectroscopic ellipsometry of graphene and an exciton-shifted van Hove peak in absorption," Phys. Rev. B **81**, 155413 (2010).
41. D. J. H. C. Maas, B. Rudin, A.-R. Bellancourt, D. Iwaniuk, S. V. Marchese, T. Südmeyer, and U. Keller, "High precision optical characterization of semiconductor saturable absorber mirrors," Opt. Express **16**, 7571-7579 (2008).
42. C. Casiraghi, A. Hartschuh, E. Lidorikis, H. Qian, H. Harutyunyan, T. Gokus, K. S. Novoselov, and A. C. Ferrari, "Rayleigh imaging of graphene and graphene layers," Nano Lett. **7**, 2711-2717 (2007).
43. W.-T. Liu, S. W. Wu, P. J. Schuck, M. Salmeron, Y. R. Shen, and F. Wang, "Nonlinear broadband photoluminescence of graphene induced by femtosecond laser irradiation," Phys. Rev. B **82**, 081408 (2010).
44. C. H. Lui, K. F. Mak, J. Shan, and T. F. Heinz, "Ultrafast Photoluminescence from Graphene," Phys. Rev. Lett. **105**, 127404 (2010).
45. M. Lazzeri, S. Piscanec, F. Mauri, A. C. Ferrari, and J. Robertson, "Electron transport and hot phonons in carbon nanotubes," Phys. Rev. Lett. **95** 236802 (2005).
46. E. Malic, T. Winzer, and A. Knorr, "Efficient orientational carrier relaxation in optically excited graphene," Appl. Phys. Lett. **101**, 213110 (2012).
47. D. Lorenser, H. J. Unold, D. J. H. C. Maas, A. Aschwanden, R. Grange, R. Paschotta, D. Ebling, E. Gini, and U. Keller, "Towards Wafer-Scale Integration of High Repetition Rate Passively Mode-Locked Surface-Emitting Semiconductor Lasers," Appl. Phys. B **79**, 927-932 (2004).
48. R. Häring, R. Paschotta, A. Aschwanden, E. Gini, F. Morier-Genoud, and U. Keller, "High-power passively mode-locked semiconductor lasers," IEEE J. of Quantum Electron. **38**, 1268-1275 (2002).

1. Introduction

Ultrafast mode-locked lasers play an increasingly important role in numerous applications, ranging from optical communications [1] to medical diagnostics [2] and industrial material processing [3]. In particular, ultrafast vertical-external-cavity surface-emitting lasers (VECSELs), also referred to as semiconductor disk lasers (SDLs) [4] or optically pumped semiconductor lasers (OPSLs) [1, 2, 4], are excellent pulsed sources for various applications, such as multi-photon microscopy [5], optical data communications [4], supercontinuum generation [6] and ultra-compact stabilized frequency combs [2,4]. In such lasers, light propagates perpendicular to the semiconductor gain layers [4]. In contrast to vertical-cavity surface-emitting lasers (VCSELs) [7], a VECSEL consists of an external cavity, formed by high-reflection mirrors, and an output coupler, with typical cavity lengths of a few mm up to tens of cm [1, 2]. The gain chip generally contains a highly reflective bottom section to reflect the laser and pump light, an active semiconductor gain section, and an anti-reflective top layer [1, 2, 4]. VECSELs combine the advantages of semiconductor lasers, such as compact footprint (down to $\sim$3 mm

#200054 - $15.00 USD Received 23 Oct 2013; revised 2 Dec 2013; accepted 2 Dec 2013; published 13 Dec 2013

cavity [8]), with those of diode pumped solid-state lasers, such as low timing jitter [9], excellent beam quality [10], high average [10, 11] and peak power [6, 12].

Currently, semiconductor saturable absorber mirrors (SESAMs) [1] are used for passive mode-locking, since they offer advantages such as an excellent ratio of saturable to non-saturable losses (e.g. 50:1 [13]) and a high damage threshold ($>0.21\,\mathrm{J/cm^2}$) [13]. However, SESAMs, epitaxially grown on lattice-matched semiconductor substrates [1], only offer a limited operation bandwidth (to date, the broadest tuning range of VECSELs mode-locked with SESAMs is 13.7 nm [14]) and have a fast recovery time ranging from several hundreds fs [15] to tens of ps [13]. Graphene, on the other hand, is the widest bandwidth material [16–18], due to the gapless linear dispersion of the Dirac electrons, and has ultrafast dynamics (<100 fs) [19, 20]. Furthermore, large-area (compared to a typical laser spot), high quality, single layer graphene (SLG) can be easily grown [21] and integrated in a variety of lasers [16, 22]. Due to its low-cost fabrication and assembly [16, 23, 24], graphene based saturable absorbers have emerged as a promising saturable absorber (SA) for ultrafast pulse generation.

The unsaturated loss (i.e. the loss of a device at low incident power) of a typical intracavity transmission device based on SLG is typically $\sim 2\times 2.3\%$ (the factor 2 accounting for the double-pass per round-trip) for the most common linear cavities [25, 26]. While this allows to use SLG as SA (GSA) to mode-lock a variety of lasers, such as fiber [23,24], solid-state [16,26] and waveguide [27], it poses serious limitations for VECSELs [2]. These typically require a SA mirror with losses $<3\%$ [28] because the small-signal gain (i.e. the optical gain for a low-intensity signal where no saturation occurs during amplification) of VECSELs suitable for mode-locking is ~ 3 to 5% [28]. Thus, inserting a SLG-based device (e.g. SLG on a quartz substrate [26]) inhibits lasing, due to the high loss induced by the $\sim 4.6\%$ absorption incurred in the double-pass per cavity round-trip.

To realize VECSEL mode-locking with graphene it is thus crucial to reduce the losses per cavity roundtrip to $<3\%$ (i.e. $<1.5\%$ for single pass) while maintaining high (in the range 0.5-2% [4]) modulation depth (i.e. the maximum absorption change induced by changing the intensity of the incident light) over a spectral range wide enough to have a sufficient modulation for the self-starting passive mode-locking of broadband VECSELs. Different methods can be used to reduce the absorption in graphene: Doping [18, 29] or gating [30] can decrease the absorption over a broad spectral range by Pauli blocking according to [18, 26]: $A(\lambda,T)=\frac{\pi^2e^2}{hc}\left[\tanh\left(\frac{\frac{hc}{\lambda}+2E_\mathrm{F}}{4k_\mathrm{B}T}\right)+\tanh\left(\frac{\frac{hc}{\lambda}-2E_\mathrm{F}}{4k_\mathrm{B}T}\right)\right]$, where T is the temperature and E_F is the Fermi level. So, e.g., to have 1.5% absorption at ~ 960 nm (the working wavelength of our laser) one would need to stably shift the Fermi level by ~ 630 meV. However, it is challenging to precisely control this high doping level. Gating usually needs extra electrical contacts and drivers, which increase the complexity of the system.

Here, we change the absorption by controlling the electric field intensity in SLG on a high-reflection mirror. The resulting SLG-based saturable absorber mirrors (GSAMs) have an unsaturated loss adjustable from 0 up to 10% and modulation depth up to 5%. These enable us to mode-lock a VECSEL, at the same time exploiting the broadband properties of graphene, thus allowing the widest wavelength-tuning thus far reported in VECSELs.

2. GSAM design and fabrication

Absorption control

The GSAM absorption is controlled as follows. The incoming and reflected waves off a mirror form a standing wave beyond the mirror surface. The field intensity enhancement $\xi(z)$ at a

#200054 - $15.00 USD Received 23 Oct 2013; revised 2 Dec 2013; accepted 2 Dec 2013; published 13 Dec 2013

distance z from the mirror can be written as [29, 31]:

$$\xi(z) = \frac{|\mathscr{E}_{\text{in}}(z) + \mathscr{E}_{\text{out}}(z)|^2}{|\mathscr{E}_{\text{in}}(z)|^2}, \tag{1}$$

where $\mathscr{E}_{\text{out}}$ and $\mathscr{E}_{\text{in}}$ are the reflected and incident wave electric fields

$$\mathscr{E}_{\text{out/in}}(z) = \mathscr{E}^0_{\text{out/in}} e^{i(\omega t \pm k_n z)}, \tag{2}$$

where $k_n = 2\pi n/\lambda$ is the wave number in the material, n is the refractive index of the material in which the light is propagating and λ is the wavelength. Based on Eq. (1), we get the field intensity enhancement ξ for an anti-resonant high-reflection ($\sim$100%) mirror with no additional coating in air:

$$\xi(z) = \frac{|\mathscr{E}_{\text{in}}(z) - \mathscr{E}_{\text{in}}(-z)|^2}{|\mathscr{E}_{\text{in}}(z)|^2} = |2i\sin(k_n z)|^2 = 4\sin^2\left(\frac{2\pi n_{\text{air}} z}{\lambda}\right), \tag{3}$$

where n_{air} is the refractive index of air. Therefore, the SLG absorption can be tuned by changing the optical distance between SLG and the mirror surface. The SLG absorption A becomes $A = \alpha\xi_{\text{abs}}$, where $\alpha \approx 2.3\%$ is the absorption of a suspended and undoped SLG [17], and ξ_{abs} is the field intensity enhancement at the absorber position. E.g., placing a SLG directly onto the mirror surface ($z = 0$ nm) we get $\xi_{\text{abs}} = 0$, thus expect no absorption due to destructive interference between incoming and reflected waves. If SLG is placed at a $\lambda/4$ distance, where there is a peak of the standing wave, we have $z = \lambda/4$ and $\xi_{\text{abs}} = 4$. Thus its absorption will increase to 400% (i.e. $4\times2.3\% \sim 9.2\%$) due to constructive interference.

For our experiment, we use SiO_2 as a spacer between the mirror surface and the SLG. Therefore, we consider the field intensity enhancement of an anti-resonant high-reflection ($\sim$100%) mirror with a SiO_2-coating of thickness d. At the air-SiO_2-interface we have [32]:

$$r_{\text{in}} = \frac{n_{\text{air}} - n_{SiO_2}}{n_{\text{air}} + n_{SiO_2}} = \frac{1 - n_{SiO_2}}{1 + n_{SiO_2}} \text{ and } r_{\text{out}} = -r_{\text{in}}, \tag{4}$$

where r_{in} and r_{out} are the Fresnel coefficients [32] of reflection at normal incidence at the air-SiO_2 and SiO_2-air interface. The corresponding Fresnel coefficients [32] for transmission at the air-SiO_2 and SiO_2-air interface are:

$$t_{\text{in}} = \frac{2n_{\text{air}}}{n_{\text{air}} + n_{SiO_2}} = \frac{2}{1 + n_{SiO_2}} \text{ and } t_{\text{out}} = \frac{2n_{SiO_2}}{n_{\text{air}} + n_{SiO_2}} = \frac{2n_{SiO_2}}{1 + n_{SiO_2}}. \tag{5}$$

The electric field of the reflected beam consists of the superposition of the incoming beam ($\mathscr{E}^{\text{in}}_{\text{air}}$) reflected at the air-$SiO_2$ interface, and the electric field of the beam ($\mathscr{E}^{\text{out}}_{SiO_2}$) transmitted in SiO_2 at the same interface:

$$\mathscr{E}^{\text{out}}_{\text{air}} = r_{\text{in}}\mathscr{E}^{\text{in}}_{\text{air}} + t_{\text{out}}\mathscr{E}^{\text{out}}_{SiO_2}, \tag{6}$$

whereas the electric field of the incident beam in SiO_2 at the interface is:

$$\mathscr{E}^{\text{in}}_{SiO_2} = t_{\text{in}}\mathscr{E}^{\text{in}}_{\text{air}} + r_{\text{out}}\mathscr{E}^{\text{out}}_{SiO_2} \tag{7}$$

and the electric field of the reflected beam in SiO_2 at the interface is:

$$\mathscr{E}^{\text{out}}_{SiO_2} = r_{\text{mirror}} e^{2in_{SiO_2}k_0 d}\mathscr{E}^{\text{in}}_{SiO_2}. \tag{8}$$

From Eqs. (7) and (8) we get with normalization of the incoming field ($\mathscr{E}^{\text{in}}_{\text{air}} = 1$):

$$\mathscr{E}^{\text{in}}_{SiO_2} = \frac{t_{\text{in}}}{1 + r_{\text{out}} e^{2in_{SiO_2}k_0 d}} \tag{9}$$

#200054 - $15.00 USD Received 23 Oct 2013; revised 2 Dec 2013; accepted 2 Dec 2013; published 13 Dec 2013

and

$$\mathscr{E}^{\text{out}}_{\text{SiO}_2} = \frac{-t_{\text{in}} e^{2in_{\text{SiO}_2}k_0 d}}{1 + r_{\text{out}} e^{2in_{\text{SiO}_2}k_0 d}}. \tag{10}$$

Inserting Eq. (10) in Eq. (6) we get the electric field of the reflected beam in air:

$$\mathscr{E}^{\text{out}}_{\text{air}} = r_{\text{in}} + t_{\text{out}} \frac{-t_{\text{in}} e^{2in_{\text{SiO}_2}k_0 d}}{1 + r_{\text{out}} e^{2in_{\text{SiO}_2}k_0 d}}. \tag{11}$$

inserting Eqs. (4), (5) and (11) in Eq. (1) we get:

$$\xi(d_{\text{SiO}_2}) = \left| 1 - \frac{4n_{\text{SiO}_2}}{(1+n_{\text{SiO}_2})^2} \frac{1}{e^{2in_{\text{SiO}_2}k_0 d} + \frac{n_{\text{SiO}_2}-1}{n_{\text{SiO}_2}+1}} + \frac{1-n_{\text{SiO}_2}}{1+n_{\text{SiO}_2}} \right|^2 \tag{12}$$

which gives the field intensity enhancement ξ at the top SLG layer of our GSAMs:

$$\xi_{\text{abs}}(d_{\text{SiO}_2}) \approx \frac{4}{1 + n^2_{\text{SiO}_2} \cot^2\left(\frac{2\pi}{\lambda} n_{\text{SiO}_2} d_{\text{SiO}_2}\right)}. \tag{13}$$

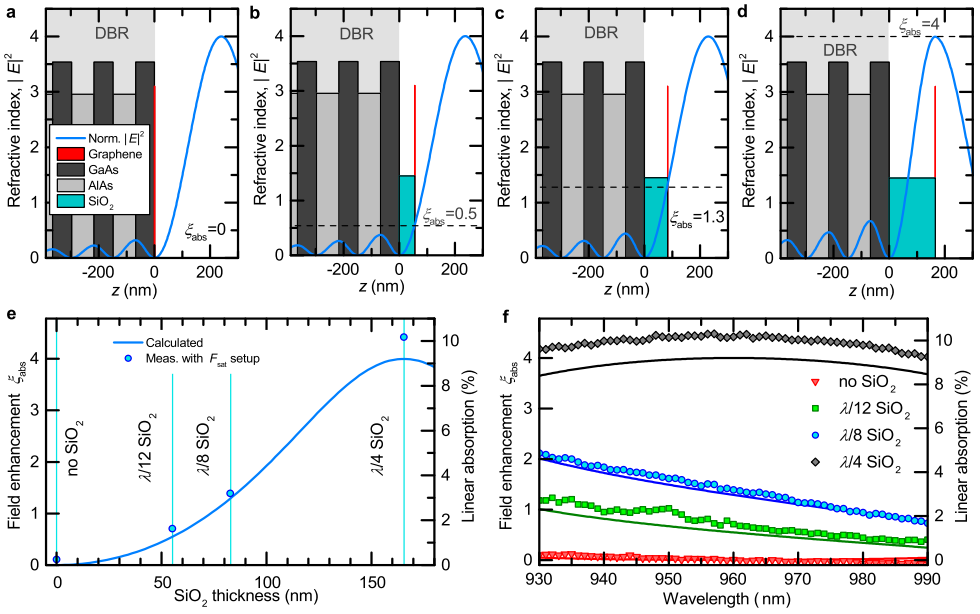

Fig. 1. **DBR-GSAM design**. Schematic zoom into the last mirror pairs with (a) no SiO_2, (b) $\lambda/12$ (55 nm) SiO_2, (c) $\lambda/8$ (83 nm) SiO_2 and (d) $\lambda/4$ (165 nm) SiO_2. The blue curve represents the normalized standing electric field intensity resulting from the refractive index profile, as a function of the vertical distance from the mirror, for the design wavelength λ=960 nm. A SLG is placed as the last layer. (e) (right axis) linear absorption and (left axis) field intensity enhancement at the SLG location corresponding to the DBRs without SiO_2 (ξ_{abs}=0), a $\lambda/12$ layer of SiO_2 (ξ_{abs}=0.5), a $\lambda/8$ layer (ξ_{abs}=1.3) and a $\lambda/4$ layer (ξ_{abs}=4). (f) (lines) calculated and (dots) experimental ξ_{abs} and absorption of the four designs as a function of wavelength.

#200054 - $15.00 USD Received 23 Oct 2013; revised 2 Dec 2013; accepted 2 Dec 2013; published 13 Dec 2013

Mirror preparation

We fabricate four GSAMs with different optical distances by coating the mirror with: 0, $\lambda/12$ SiO_2, $\lambda/8$ SiO_2 and $\lambda/4$ SiO_2. We use anti-resonant distributed Bragg reflectors (DBRs) [31,33] as high-reflection mirrors. These typically consist of a stack of multiple layers with alternating high and low refractive index [31,33], each with an optical thickness of a quarter of the design wavelength. The partial reflections at the layer interfaces can interfere constructively resulting in high reflection ($\sim$100% [31,33]). Our 30-pair anti-resonant AlAs/GaAs (81.1 nm/67.85 nm) DBRs are grown on a 600 μm thick GaAs substrate by molecular beam epitaxy (MBE, VEECO GEN III). They are designed to give a node of the standing wave at the surface of the top layer (anti-resonance), with reflectivity >99.997% at 960 nm (our VECSELs wavelength). Subsequently, the wafer is cleaved into 1×1 cm^2 pieces and then coated by plasma enhanced chemical vapor deposited (Oxford Instruments PECVD 80+) SiO_2 with different thickness (d_{SiO_2}): 0, $\lambda/12$, $\lambda/8$ and $\lambda/4$, i.e 0, 55, 83 and 165 nm. According to Eq. (13), this gives a field intensity enhancement ξ_{abs} of 0, 0.5, 1.3 and 4 respectively. The layer thickness of the SiO_2 is measured on reference Si samples with an ellipsometer. Figures 1(a)–1(d) plot schematics of the DBR.

Graphene fabrication and transfer

SLG is then grown by CVD [34] by heating a 35 μm thick Cu foil to 1000^{o}C in a quartz tube, with 10 sccm H_2 flow at $\sim5\times10^{-2}$ Torr. The H_2 flow is maintained for 30 min in order to reduce the oxidized Cu surface [21,34] and to increase the graphene grain size [21,34]. The precursor gas, a H_2:CH_4 mixture with flow ratio 10:15, is injected at a pressure of 4.5×10^{-1} Torr for 30 min. The carbon atoms adsorb onto the Cu surface and form SLG via grain propagation [21, 34]. A 5×5 mm^2 SLG is transferred onto the SiO_2-coated mirrors as follows [21, 26]: First, a layer of poly(methyl meth-acrylate) (PMMA) is spin-coated on the samples. The Cu foil is etched using a mixture of 3% H_2O_2: 35% HCl (3:1 ratio), which is further diluted in equal volume of deionized water. The PMMA/graphene films are then rinsed in two consecutive deionized H_2O baths. Next, the films are picked up on the mirror substrates and left to dry under ambient conditions. Finally, the PMMA is dissolved in acetone, leaving the SLG films on the mirrors.

3. GSAM characterization

Raman spectroscopy

The quality of graphene before and after transfer is monitored by optical microscopy, absorption spectroscopy and Raman spectroscopy (Renishaw InVia micro-Raman spectrometer equipped with a Leica DM LM microscope and a 100X objective) [35–37]. The Raman spectrum before transfer is shown in Fig. 2(a). This is measured at 457 nm excitation, since this wavelength suppresses the Cu luminescence, which would result in a non-flat background [26]. The spectrum shows a very small I(D)/I(G)$\approx$0.004, indicating negligible defects [35–38]. The 2D peak is a single sharp Lorentzian with full width at half maximum, FWHM(2D)$\sim$35 cm^{-1}, a signature of SLG [35]. Representative Raman spectra of the transferred graphene on the 0, $\lambda/4$ SiO_2, $\lambda/8$ SiO_2, $\lambda/12$ SiO_2 devices are shown in Fig. 2(a). After transfer, the 2D peak is still a single sharp Lorentzian with FWHM(2D)$\sim$35 cm^{-1}, confirming that SLG has indeed been successfully transferred, and I(D)/I(G)$\sim$0.005, showing that negligible additional defects are induced by the transfer process. In order to estimate the doping level of the transferred films, an analysis of more than 10 measurements is carried out for 514 nm excitation. We use this wavelength as most previous literature and correlations were derived at 514 nm [39]. For the film transferred on the $\lambda/8$ SiO_2 sample, the average G peak position, Pos(G), and FWHM(G), are 1591.8 cm^{-1} and 14.6 cm^{-1}. The average Pos(2D) is 2693 cm^{-1}, and the 2D to G intensity and area ratios

#200054 - $15.00 USD Received 23 Oct 2013; revised 2 Dec 2013; accepted 2 Dec 2013; published 13 Dec 2013

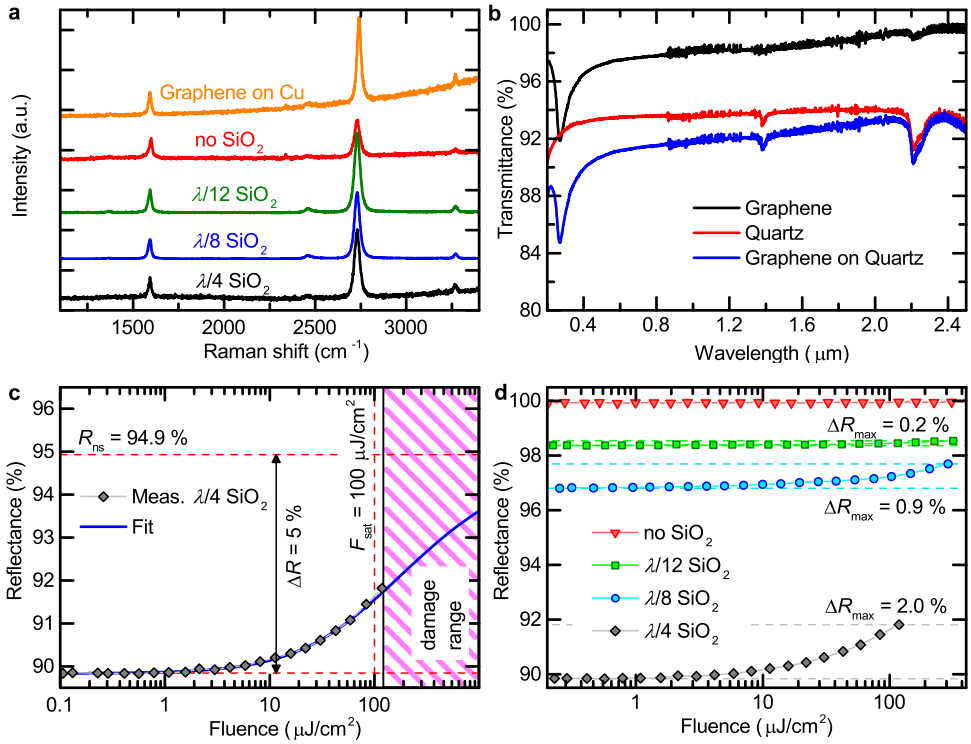

Fig. 2. **Raman characterization and non-linear response**. (a) Raman spectra of graphene on Cu and after transfer on the no-SiO_2, $\lambda/4$ SiO_2, $\lambda/8$ SiO_2, $\lambda/12$ SiO_2 devices. (b) Transmittance of the same graphene transferred on a quartz substrate, derived from the transmittance of transferred graphene on quartz divided by that of quartz. (c) Non-linear reflectivity of the $\lambda/4$ SiO_2 sample (black markers) and fit assuming a 5% saturable and 5.1% non-saturable absorption (blue curve), resulting in a saturation fluence of 100 μJ/cm^2. (d) Non-linear reflectivity of all GSAMs.

I(2D)/I(G); A(2D)/A(G), are 2.7 and 6.3. This indicates a p-doping $\sim 0.5\times 10^{13}\,\mathrm{cm}^{-2}$, corresponding to a Fermi level shift $\sim$300 meV [39]. Similarly, for the $\lambda/4$- and $\lambda/12$-mirrors we get a p-doping $\sim 0.8\times 10^{13}\,\mathrm{cm}^{-2}$, corresponding to a Fermi level shift $<$400 meV. For comparison, we also transferred SLG on quartz, Fig. 2(b). The band at $\sim$0.270 μm is a signature of the van Hove singularity in the graphene density of states [40], while those at $\sim$1.4 and 2.2 μm are due to the quartz substrate [26]. The absorption at 960 nm (our operation wavelength) is $\sim$2.3%, decreasing to $\sim$1% at 2 μm due to doping [18,26]. By fitting to the measured transmittance ($T_r \approx 1-A$), we get $E_F \sim$350 meV, consistent with the Raman estimates. However, such doping level is not enough to significantly affect the absorption at 960 nm, which is $\sim$2.3% as for intrinsic SLG [17, 18].

Linear absorption

The linear unsaturated absorption of our four GSAMs at 960 nm, measured with a high-precision (0.05% resolution) reflectivity setup [41] is plotted in Fig. 1(e). This also shows the calculated absorption from Eq. (13). Our devices have A=0.25%, 1.6%, 3.2% and 10% at 960 nm, in agreement with calculations. Figure 1(f) reports the field intensity enhancement calculated from Eq. (13) as a function of wavelength, compared to experiments. This further

#200054 - $15.00 USD Received 23 Oct 2013; revised 2 Dec 2013; accepted 2 Dec 2013; published 13 Dec 2013

validates the results. Note that the absorption is not flat as that of graphene on quartz, see Fig. 2(b), because ξ depends on the wavelength according to Eq. (13), as shown in Fig. 1(f).

Non-linear absorption

We also characterize the GSAMs reflectivity as a function of input light fluence (J/cm^2) using the high-precision reflectivity setup described in [41]. A Kerr-lens mode-locked Ti:Sapphire laser (Tsunami, Spectra-Physics) is used as a probe laser, with 100 fs pulse duration at a 80 MHz repetition rate, with ~740 mW average power at 960 nm. The fluence-dependent reflectivity measurements (non-linear reflectivity) show an increase in reflectivity with fluence as expected from a SA, Fig. 2(d). The maximum changes in reflectivity for $\lambda/12$, $\lambda/8$ and $\lambda/4$ devices are 0.2%, 0.9% and 2%. The measurement for the $\lambda/4$ SiO_2 device (i.e. the sample with ξ=4 at the graphene position) is shown in Fig. 2(c). For a fast SA (i.e. where the absorber recovery time is faster than the probe pulse duration), the reflectivity can be written as [29]:

$$R(F) \approx \frac{R_{\mathrm{lin}} - R_{\mathrm{ns}}}{\sqrt{\frac{F}{F_{\mathrm{sat}}} + \left(\frac{F}{F_{\mathrm{sat}}}\right)^2}} \operatorname{atanh}\left[\sqrt{\frac{F}{F_{\mathrm{sat}} + F}}\right] + R_{\mathrm{ns}}, \tag{14}$$

where R_{lin} is the unsaturated reflectivity, R_{ns} the non-saturable reflectivity, F_{sat} the saturation

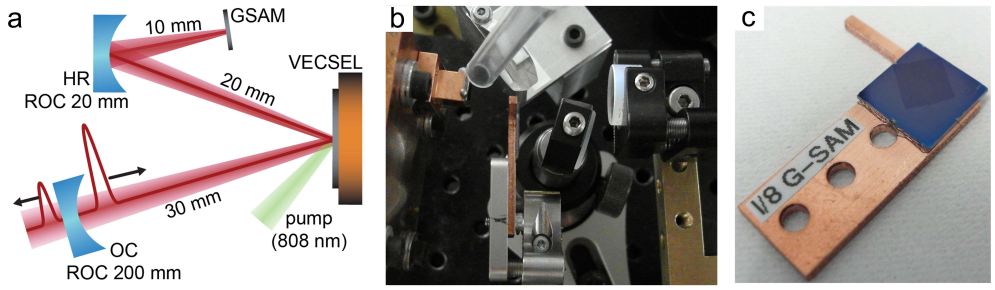

Fig. 3. **Laser setup**. (a) Schematic of the VECSEL setup. OC: output coupler mirror. HR: high reflective folding mirror. GSAM: graphene saturable absorber. The VECSEL gain chip is placed as a folding mirror and pumped under a 45^o angle. The total cavity length is 6 cm. (b) Picture of the laser setup. (c) Picture of the $\lambda/8$ GSAM. The SLG is clearly seen as shaded area, since the 83 nm SiO_2 thickness gives a a high optical contrast in the visible range [42].

fluence. We estimate a saturation fluence F_{sat} ~100 μJ/cm^2 (corresponding to a peak intensity I_{peak} ~1.0 GW/cm^2), as extracted by fitting Eq. (14) to the data in Fig. 2(c). The estimated modulation depth is ~5%, 2.7 times larger than that reported for SLG on quartz [25]. When a higher input fluence (>120 μJ/cm^2 (4 GW/cm^2)) is used, the GSAM reflectivity starts to increase permanently, indicating degradation. From Eq. (14), the F_{sat} of the $\lambda/8$ sample is estimated as ~200 μJ/cm^2, higher than the $\lambda/4$ sample, because the smaller field intensity enhancement at the absorber makes the device saturate at a higher fluence. In this case, degradation also starts at higher fluence (>300 μJ/cm^2). In SLG, the non-equilibrium (non-thermal) distribution of electrons in conduction band and holes in valence band created by an ultrafast pulse relaxes, eventually reaching thermal equilibrium with the lattice, due to various processes [19,20], including carrier-carrier and carrier-phonon scattering, as well as radiative electron-hole recombination (non-linear photoluminescence [16, 43, 44]). In the sub-ps time-frame two main processes occur: first, the initial peak produced by the pump laser broadens, due to carrier-carrier collisions, converging towards a hot Fermi-Dirac shape on an ultrashort time scale <100 fs [19, 20]. On

#200054 - $15.00 USD Received 23 Oct 2013; revised 2 Dec 2013; accepted 2 Dec 2013; published 13 Dec 2013

a longer timescale, optical phonon emission [45] drives a cooling in which the Fermi Dirac distribution shifts towards the Dirac point [19, 20, 46].

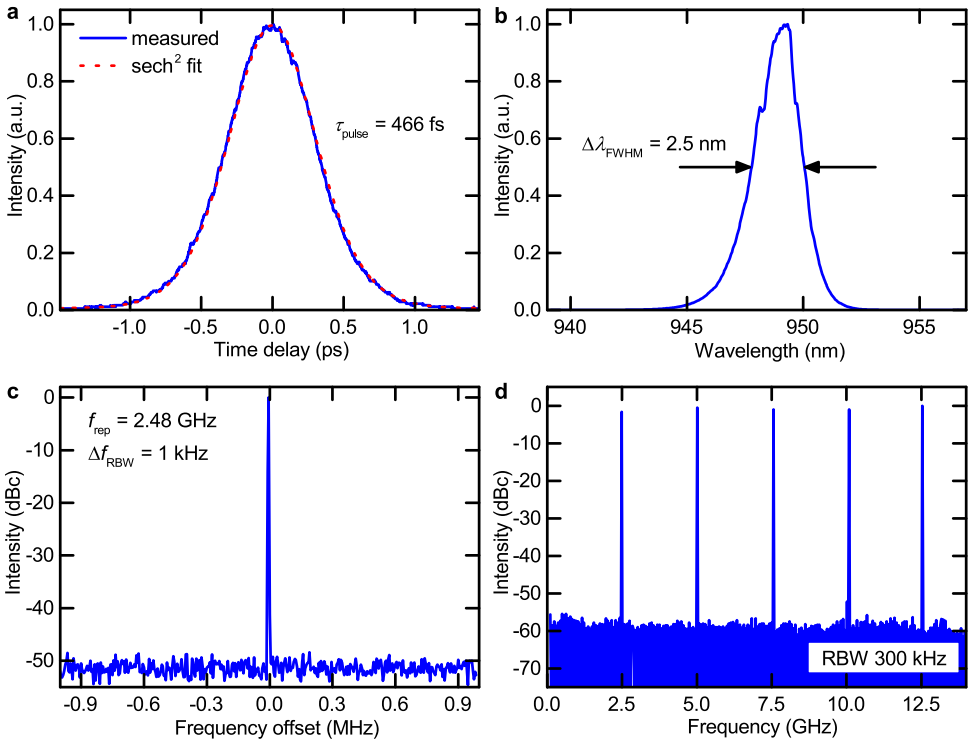

Fig. 4. **Mode-locking results**. (a) (Blue line) second harmonic autocorrelation signal and (dashed red line) fit with the autocorrelation of an ideal sech^2-shaped pulse, corresponding to a pulse duration of 466 fs. (b) Optical spectrum. (c) Microwave spectrum centered around the repetition rate of 2.5 GHz, measured with a 1 kHz resolution bandwidth (RBW). (d) Microwave spectrum measured from 0 to 13 GHz with RBW=300 kHz, showing the first 5 harmonic peaks of the repetition rate (f_{rep}).

4. Mode-locking results

For VECSEL mode-locking we select the $\lambda/8$ GSAM because it offers suitable linear loss (<3%). This device also provides a larger modulation depth (> 0.9%) compared to the $\lambda/12$ GSAM. The laser cavity configuration is sketched in Fig. 3(a), with a picture in Fig. 3(b). The resonator mode and pump spot radius on the gain chip are 150 μm. In order to achieve a sufficient intensity to saturate the GSAM, we implement a beam waist $\sim$30 μm on the absorber using a concave folding mirror with a 20 mm radius of curvature. A picture of the $\lambda/8$-GSAM is shown in Fig. 3(c).

We use three different VECSEL gain chips: Two QW VECSELs emitting at $\sim$940 and 970 nm are grown by metal-organic vapor phase epitaxy (MOVPE, AIXTRON AIX 200/4) as described in [47]. A QD VECSEL with an emission wavelength $\sim$950 nm is grown by MBE as described in [15]. Instead of 9 QD layers placed in 7 subsequent anti-nodes of the electric field as in [47], our gain chip has 2x9 QD layers placed in the first anti-node, whereas no QDs are placed in the 6th anti-node, so to balance the stronger excitation due to higher absorption of

#200054 - $15.00 USD Received 23 Oct 2013; revised 2 Dec 2013; accepted 2 Dec 2013; published 13 Dec 2013

the pump light around the first anti-nodes. All gain structures are grown in reverse order, and subsequently processed on a diamond heat sink grown by CVD as described in [48]. The pump laser is coupled into a 200 μm fiber.

Using the gain chip optimized for ~950 nm, we obtain stable mode-locking with a pulse duration of 466 fs, measured with an intensity autocorrelator (Femtochrome FR103XL) as shown in Fig. 4(a). The spectrum is centered at ~949 nm with FWHM=2.5 nm, Fig. 4(b), as analyzed with an optical spectrum analyzer (HP 70952). Note that the field intensity enhancement of our $\lambda/8$ GSAM is ξ_{abs}=1.5 at 949 nm compared to 1.3 at 960 nm, see Fig. 1(f). The pulse repetition rate is 2.5 GHz, detected with a fast photodiode (New Focus 1434) and measured with a microwave spectrum analyzer (MSA, HP 70952), see Fig. 4(c) and 4(d), one order of magnitude higher than previous fiber [22,24] and solid-state [22,26] lasers mode-locked by graphene, due to the compactness of our VECSEL design. The time-bandwidth product is 0.353, 1.1 times larger than what expected for transform-limited sech^2 pulses, indicating that the output pulses are slightly chirped (i.e. the instantaneous frequencies are time-dependent [32]). The average output power is 12.5 mW, with a 0.2% output coupling (OC) transmission. Higher power up to 26 mW with 2 ps pulses is also achieved using a 0.5% OC transmission. We calculate the input pulse fluence on the GSAM as ~125 μJ/cm^2, corresponding to a reflectivity modulation of ~0.55%, according to Fig. 2(a). We did not observe any degradation of the GSAM for several hours operation.

In order to verify the broadband operation of our GSAM, we also perform a wavelength-

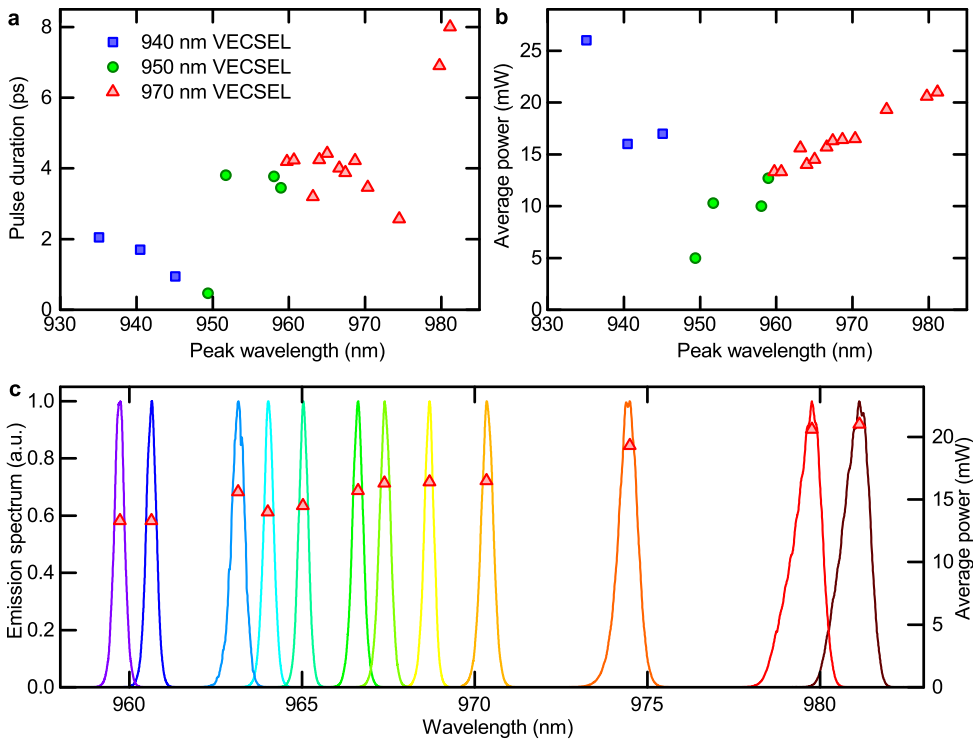

Fig. 5. **Tuning results**. Mode-locking with the $\lambda/8$ GSAM in VECSELs optimized for different emission wavelengths. An intra-cavity etalon is used, except for the two points at 935 and 949 nm. (a) Pulse duration and (b) average output power at different emission wavelengths. (c) Emission spectra for the 970 nm-VECSEL and average output power.

#200054 - $15.00 USD Received 23 Oct 2013; revised 2 Dec 2013; accepted 2 Dec 2013; published 13 Dec 2013

tuning study using the VECSELs described above. We use a $\sim$10 cm cavity at 1.5 GHz, with various OC transmission rates and gain chips to fully test our GSAMs. A Fabry-Pérot fused silica etalon (20 μm thick) is used for wavelength tuning. In order to optimize the output power at a given emission wavelength, the gain chip heat sink temperature is adjusted between -20 and +20^{o}C. Mode-locked operation is obtained in a range from 935 to 981 nm (46 nm), with pulse durations up to 8 ps as shown in Fig. 5(d). Figures 5(a) and 5(b) show the pulse duration and average output power for different emission wavelengths. A maximum tuning range of 21 nm with a single VECSEL gain chip is achieved with the 970 nm QW VECSEL, Fig. 5(c). This is larger than previously reported with any SESAM mode-locked VECSEL [14].

5. Conclusions

We demonstrated a versatile approach to engineer the absorption of graphene saturable absorber mirrors in the 0-10% range. Accordingly, the saturation fluence can be adjusted with the field intensity enhancement. We mode-locked VECSELs with a series of different gain chips over a 46 nm wavelength range (from 935 to 981 nm) with repetition rates up to 2.48 GHz, and 466 fs pulse duration. This can lead to novel graphene based ultrafast light sources to meet the wavelength range, repetition rate and pulse duration requirements for various applications (e.g. metrology, spectroscopy and data-communication).

Acknowledgments

We thank Prof. T. Südmeyer for useful discussions. We acknowledge funding from a Royal Society Wolfson Research Merit Award, the European Research Council Grants NANOPOTS, Hetero2D, EU grants RODIN, GENIUS, MEM4WIN, CareRAMM, and Graphene Flagship (contract no. NECT-ICT-604391), EPSRC grants EP/K01711X/1, EP/K017144/1, EP/G042357/1, Nokia Research Centre, Emmanuel College, Cambridge, the FIRST clean room facility of ETH, the Swiss National Science Foundation (SNSF) and the Swiss Confederation Program Nano-Tera.ch, which was scientifically evaluated by the SNSF.

#200054 - $15.00 USD Received 23 Oct 2013; revised 2 Dec 2013; accepted 2 Dec 2013; published 13 Dec 2013